Journal of Power Sources

Submitted October 14, 2013

(Revised) December 16, 2013

# Characterization of as-deposited $Li_4Ti_5O_{12}$ thin film electrode prepared by aerosol deposition method

Ryoji Inada*, Kenta Shibukawa, Chiaki Masada, Yuta Nakanishi, and Yoji Sakurai

Department of Electrical and Electronic Information Engineering, Toyohashi University of Technology, 1-1 Hibarigaoka, Tempaku-cho, Toyohashi, Aichi 441-8580, Japan.

*Corresponding author

Ryoji Inada, Associate Professor

Postal address: Toyohashi University of Technology, 1-1 Tempaku-cho, Toyohashi, Aichi 441-8580, Japan

Phone: +81-532-44-6723

Fax: +81-532-44-6757

E-mail address: inada@ee.tut.ac.jp

**Abstract**

We successfully fabricated lithium titanate $Li_4Ti_5O_{12}$ (LTO) thin film electrode at room temperature by aerosol deposition (AD) method. Agglomerated LTO powder with the size of 5–6 μm composed of primary sub-micron particles was used as raw material and deposited directly on a stainless steel substrate via room temperature impact consolidation (RTIC). X-ray diffraction patterns revealed that as-deposited LTO film has a same crystalline structure with raw powder and no secondary phases were formed during the deposition process. SEM observation showed that the film has porous structure consisted from LTO particles with the sizes of several 100 nm. As-deposited LTO film electrode showed good electrochemical property in liquid electrolyte. The discharge capacities of 159 mAh $g^{-1}$ and 125 mAh $g^{-1}$ were obtained at current density of 0.067 mA $cm^{-2}$ (= 0.5C rate) and 2.68 mA $cm^{-2}$ (= 20C rate). The former corresponds to 91% of theoretical capacity for LTO (= 175 mAh $g^{-1}$). The film electrode also showed good capacity retention, indicating that adhesion between the film and substrate are sufficiently strong.

**Keywords:** Aerosol deposition, $Li_4Ti_5O_{12}$, film electrode, electrochemical property

## 1. Introduction

All solid state thin film lithium-ion battery is a promising next generation battery system for RFID tags, smart cards, and other low power portable devices because of its high safety, reliability and long cycle stability [1–4]. Thin film electrodes can be prepared with pulsed laser deposition (PLD) [5–11], sputtering deposition [12–18], and electrostatic spray deposition (ESD) [19–21]. These methods are efficient for fabrication of uniform film and controlling the film thickness, but in some cases, it is difficult to control stoichiometric composition of the as-designed thin film [8, 13]. Moreover, increasing the substrate temperature during deposition and/or post-annealing should be necessary to obtain well-crystallized thin films [5–21]. Since high temperature treatments may lead to undesired reactions at the interface or uncontrolled diffusion, this process is not recommended in many cases, making this conventional method inadequate in fabrication of all-solid-state batteries.

Aerosol deposition (AD) has many advantages compared to the conventional thin film deposition methods as mentioned above, including the deposition of a crystallized thin film without any heat treatment and a fast deposition rate [22–24]. A thin film is deposited through impact and adhesion of fine particles on substrate by the pressure difference at room temperature. This unique phenomenon was called as “room temperature impact consolidation (RTIC)”. The film consequently has the characteristic properties of the powder material, such as the crystal structure, composition and physical property. AD additionally provides a number of advantages, including room temperature deposition and high adhesion strength with the substrate [22–24]. By addressing these attractive features, numerous studies to form thin film by using AD method have been reported in various functional ceramic materials, including

$Pb(Zr,Ti)O_3$ (PZT) [23, 24], $(K_{0.5}Na_{0.5})NbO_3$ [25], $TiO_2$ [26], and $Ca_3Co_4O_9$ films [27]. Several related papers have been also reported in the battery field. Popovici et al. reported the adoption of AD to prepare $Li_{1.3}Al_{0.3}Ti_{1.7}(PO_4)_3$ (LATP) solid electrolyte film [28]. The electrochemical properties of Si alloy or composite [29–32], $LiMnO_2$ [33], $LiNi_{0.4}Co_{0.3}Mn_{0.3}O_2$ [34] and $LiFePO_4$ [35] thin film electrodes were also investigated to verify the feasibility of AD. Although the film electrodes formed by AD show excellent cycle stability, the specific charge and discharge capacities of the as-deposited film electrodes are 30–40% smaller than the theoretical one [33–35]. This might be related to severe strain and degraded crystallinity in the film by AD. During deposition, the initial particles fracture into fine grains of several tens nanometer size and deposit on the substrate [22, 28, 33–35] and these fine grains have severe strain. This has been confirmed in X-ray diffraction patterns for as-deposited $Li_{1.3}Al_{0.3}Ti_{1.7}(PO_4)_3$ (LATP) [28] and $LiNi_{0.4}Co_{0.3}Mn_{0.3}O_2$ films prepared by AD [34]. In these films, not only the broadening of diffraction peaks but also the peak shift compared with their raw powders is clearly observed. The former is considered to be caused by fracturing raw powders and latter is due to the lattice distortion of crystalline particles in the film. Therefore, for practical use of AD as a fabrication method of solid state thin film battery, further study was needed to achieve high capacity in as-deposited film electrode by controlling the morphology of raw powder and deposition conditions.

In this paper, we fabricated $Li_4Ti_5O_{12}$ (LTO) film electrode by AD method. LTO is widely known to be a highly safe anode material for lithium ion batteries because it has sufficiently higher operating potential (~1.55 V) than that for lithium plating [36–38]. Since the volume change of LTO during charge and discharge is negligibly small, LTO also has an advantage not only for cycle stability but also for constituting good

electrode-electrolyte interface in solid state battery. To date, several papers have been already reported for LTO films by other fabrication method including PLD [10, 11], sputtering method [17, 18], ESD [21], sol-gel method [39, 40], and ink-jet printing [41]. Most of these LTO films have sufficiently high crystallinity via high temperature treatment and show similar charge-discharge properties and cycle stability as conventional LTO electrode with conducting additives and binder coated on the metal foil [36–38]. However, applicability of AD method for fabricating LTO film has not been fully examined. In the present work, commercially available LTO powder was directly used as raw material for fabrication of LTO film by AD method. The crystallinity, microstructure and electrochemical property of as-deposited film (without any heat treatment) were investigated.

## 2. Experimental

Commercially available $Li_4Ti_5O_{12}$ (LTO) powder (ENERMIGHT® LT-106, Ishihara Sangyo Kaisha, Ltd.) without carbon coating was directly used as a raw material for LTO film fabrication by AD [42]. Schematic illustration of AD apparatus is shown in Fig. 1. It consists of a carrier gas supply system, an aerosol chamber, and a deposition chamber equipped with a motored *X*–*Y* stage and a nozzle with a thin rectangular shaped orifice with the size of 10 mm × 0.5 mm. The deposition starts with evacuating the deposition chamber. A pressure difference between the carrier gas system and the deposition chamber is then generated as a power source for the deposition. A carrier gas flows out from the carrier gas supply system to the aerosol chamber. In the aerosol chamber, the powder is dispersed into the carrier gas with no agglomeration. Finally, the well dispersed aerosol flows into the deposition chamber through a tube and

is sprayed onto the substrate arranged on the stage. Stainless steel discs (SUS316, diameter =15.5 mm and thickness = 0.5 mm) were used as a substrate. The deposition area is masked into a circular shape with its area size of 0.5 $cm^2$ (corresponding to its diameter of 8 mm). Nitrogen gas was used as a carrier gas. The deposition chamber was evacuated to a low vacuum state of about several 10 Pa and the deposition was carried out for 20 min. During the deposition, the stage was moved uni-axially with the back-and-forth motion length of 50 mm.

For the film deposition by AD, the several conditions such as distance from the tip of nozzle, mass flow of $N_2$ carrier gas and pressure of deposition chamber during film deposition should be optimized. By using commercial LTO powders as mentioned above, we preliminary changed the pressure of deposition chamber between 0.2 and 1.2 kPa depending on the mass flow of $N_2$ carrier gas in the range of 5 to 25 L/min, while the distance between the tip of nozzle and the substrate was fixed to be 10 mm. It was confirmed that LTO film was formed on the stainless steel substrate at the pressure of deposition chamber above 0.5 kPa and the film thickness for fixed deposition time of 20 min gradually increased at the pressure of deposition chamber up to 1 kPa. Based on this result, the pressure of deposition chamber was fixed to 1 kPa. Corresponding mass flow $N_2$ carrier gas of 20 L/min. Simple tape testing was also carried out to confirm the adhesion between as-deposited LTO film and stainless steel substrate. Kapton® tape was put on to the film and then it peeled, but no exfoliation of the film from the substrate was observed.

Crystal structure of both LTO powder as a raw material and as-deposited LTO film by AD was evaluated by X-ray Diffractometer (RINT-2500, Rigaku) using CuKα radiation, with measurement range $2\theta$ = 5–90° and step interval of 0.02°. Particle size

distribution of raw LTO powder was measured by using Laser Diffraction Particle Size Analyzer (SALD-2000, Shimadzu). Field-emission scanning electron microscope (FE-SEM, SU8000 Type II, Hitachi) was used to observe the microstructure of raw LTO powder and as-deposited LTO film.

As-deposited LTO film on stainless steel substrate was investigated by using two-electrode set up. LTO film is used as working electrode, where as a single lithium foil serve as both counter and reference electrodes. The electrolyte solution was 1 mol $LiPF_6$ in a mixture or ethylene carbonate (EC) and dimethyl carbonate (DMC) with a volume ratio of 1:1 (Kishida Chemical Co., Ltd.). Together with Celgard 3501 as a separator, these components were assembled in a CR2032 coin type cell. The assembly of the cell was carried out in a dry Argon-filled glove box (UN-650FCH, UNICO). The cells was charged and discharged over a voltage range between 1.2 and 2.5 V versus $Li/Li^+$ electrode at different fixed current density of 0.067, 0.134, 0.268, 0.536, 1.34 and 2.68 mA $cm^{-2}$ and 20°C using Battery Test System (TOSCAT-3100, TOYO-SYSTEM).

## 3. Results and discussion

It is known that both morphology and particle size of the raw material are important factors for AD [22]. Fig. 2 shows the SEM image of commercial LTO powder used as a raw material for LTO film by AD. It is confirmed that primary LTO particles with the size of several 100 nm agglomerate and constitute a sphere shaped secondary particle with the size of 5–7 μm. Measured particle size distribution of LTO powder is also shown in Fig. 3. Averaged particle size is corresponding to the size of secondary agglomerated particle shown in Fig. 2.

XRD patterns for LTO powder used as raw material and as-deposited LTO film on

stainless steel substrate are compared in Fig. 4. It is noted that the absolute value for peak intensity in raw LTO powder is approximately six times larger than that for LTO film by AD. As can be seen, LTO powder used as raw material has cubic spinel structure with a space group *Fd*-3*m*. The peaks from LTO with cubic spinel structure are clearly confirmed in as-deposited LTO thin film, together with the peak from stainless steel substrate. This indicates that crystalline LTO film can be successfully fabricated at room temperature condition. The peaks from other phases were not observed. This feature is a significant advantage over other conventional thin film deposition methods such as PLD and sputtering, because by using these deposition methods, heat treatment such as heating substrate during deposition or post annealing should be necessary to obtain the well crystallized film [5–21].

Fig. 5 is the comparison of the enlarged (111) diffraction peaks of the raw LTO powder and as-deposited LTO film. As can be seen, full width of half maximum (FWHM) of the peak was estimated to be 0.16° and 0.18° for raw powder and as-deposited film, respectively. The deviation of 0.02° is corresponding to twice the measuring step (= 0.02°) of XRD patterns, so that the deviation is within the level for measurement error and the sharpness of diffraction peak for raw powder and as-deposited film is nearly identical. This feature was also confirmed in other diffraction peaks, indicating that the crystallinity of as-deposited LTO film is as high as raw LTO powders, but quite different from other ceramic films formed by AD [23–28, 34, 35]. It has been reported that the diffraction peaks for most of as-deposited film fabricated by AD method are broadened and the peak intensity is lowered significantly. This is closely related with the deposition mechanism of AD. During the deposition, the initial particles fracture into fine grains of several tens nanometer size and deposit on the substrate.

Moreover, these fine grains have severe strain and lower crystallinity than raw powders, which is observed as the shift of diffraction peaks as mentioned above [34]. However, the diffraction peaks for our LTO film are not broadened and peak shift is not observed, compared with those for raw powders. These results suggest that the fractured LTO particle in the film is not damaged and has no strain by the impact during the deposition.

Fig. 6 shows the SEM image of the fractured cross section for as-deposited LTO film on stainless steel substrate. As can be seen, LTO film was successfully deposited on the stainless steel substrate at room temperature condition. Film surface seems to be very rough. It was confirmed that as-deposited LTO film has a little porous structure and the film thickness is confirmed to be approximately 3.0–3.3 μm. Film density was calculated by using physical dimension and weight of the film (= 0.42 mg). Relative density (normalized by theoretical crystalline density of LTO = 3.5 $gcm^{-3}$) was estimated to be approximately 75–80%. This is consistent with a microstructure of as-deposited LTO film in Fig. 6. The size of LTO particle in as-deposited film seems to be several 100 nm, which is very close to the primary particle size in raw LTO powders as shown in Fig. 2. This suggests that agglomerated secondary LTO particles were fractured by impact at the deposition, but most of primary LTO particles were not fractured and connected each other to form the film. The fact that the diffraction peaks of LTO film were not broadened compared with raw LTO powders (shown in Fig. 5) supports this speculation indirectly. In addition, XRD data of LTO film does not have any peak shift compared with raw LTO powder, indicating that the film seems to be free of strain. This feature is quite different from those for the film fabricated by AD as previously reported [23–28, 34, 35]. For instance, both the broadening of diffraction peaks but also the peak shift compared with their raw powder are clearly confirmed in

the XRD patterns for as-deposited $LiNi_{0.4}Co_{0.3}Mn_{0.3}O_2$ (LNCMO) film by AD [34]. In this film, well dispersed primary LNCMO particles with the averaged size of 1 μm are used as raw materials and strongly fractured into fine particles with the size of several 10 to 100 nm during deposition process. In addition, (003) peak of LNCMO is emphasized in as-deposited film and shifted toward higher angle compared with raw LNCMO powder, indicating that c-axis of LNCMO is oriented in perpendicular to film surface and the reduction of lattice parameter along *c*-axis of LNCMO. These results suggest that the film has severe strain due to strongly fractured primary particles. At present stage, the origin to cause the difference in the degree in fracture of primary particle in AD method has not been clarified yet, but it might be related with the structure and the size of raw agglomerated LTO powder we used. Further investigation for the influence of the morphology and the size of raw powder on the crystallinity and microstructure in as-deposited film by AD should be necessary in future.

The initial charge–discharge curves of as-deposited LTO film electrode by AD at 20°C and various current densities per unit-electrode area from 0.067 to 2.68 mA $cm^{-2}$ are summarized in Fig. 7. At low current density of 0.067 mAh $g^{-1}$, the charge and discharge curves show the plateau regions between 1.5 and 1.6 V vs $Li/Li^+$. The profile is quite similar to that for conventional coated LTO electrode with conducting additives and binder on the metal foil [36–38]. Though as-deposited film does not contain any conducting additives, the discharge capacities of 159 mAh $g^{-1}$ and 125 mAh $g^{-1}$ (corresponding to 0.13 mAh $cm^{-2}$ and 0.10 mAh $cm^{-2}$) were obtained at current density of 0.067 mA $cm^{-2}$ (= 0.5C) and 2.68 mA $cm^{-2}$ (= 20C), respectively (1C = 0.134 mA $cm^{-2}$). Each discharge capacity at 0.5C and 20 C rate are approximately 91% and 74% of the theoretical capacity of LTO (= 175 mAh $g^{-1}$). Rate capability of discharge

capacity of the LTO film electrode is also shown in Fig. 8. It is confirmed that comparing with the discharge capacity at 0.5C (= 159 mAh $g^{-1}$), as-deposited LTO film electrode shows capacity retention of 97%, 94%, 87% and 79% at high C-rate of 2C, 4C, 10C and 20C.

Such good electrochemical properties of LTO film by AD could be attributed to both the microstructure and the crystallinity. As shown in Fig. 6, the film has a little porous structure, which is favorable for percolation of liquid electrolyte into the film and formation of good electrode-electrolyte interface for $Li^+$ insertion and extraction. Moreover, as expected from Fig. 5 and Fig. 6, the LTO particle consisting the film are expected to be not damaged so much during the impact consolidation on the stainless substrate. Consequently, the crystallinity of our LTO film is nearly the same as raw LTO powders. In $LiMnO_2$ [29], $LiNi_{0.4}Co_{0.3}Mn_{0.3}O_2$ [30] and $LiFePO_4$ [31] film electrodes formed by AD, the specific capacities of the as-deposited films are reported to be 30–40% smaller than the theoretical ones. One of the main reasons of such a deteriorated electrochemical property of these films is considered to be the degradation of crystallinity of the film due to the strain introduction via impact consolidation [29–31].

Cycle stability for both discharge capacity and coulombic efficiency of as-deposited LTO film are shown in Figs. 9 and 10 at different fixed current density at both charge and discharge of 0.134 mA $cm^{-2}$ (= 1C) and 0.536 mA $cm^{-2}$ (= 4C). It is noted that the measurement at 4C was carried out after finishing the measurement at 1C. As can be seen, as-deposited LTO electrode showed excellent cycle stability during 100 cycles at each current density. Capacity retention after 100 cycles was confirmed to be above 98% at 1C and 96% at 4C, respectively. The coulombic efficiency was nearly

equal to 100% excepting first cycle, which indicates that the reversibility of $Li^+$ insertion and extraction into LTO film was good. Such excellent cycle stability of LTO film electrode fabricated by AD is attributed to not only high durability of LTO itself but also sufficiently strong adhesion between the film and substrate.

To control the morphology and density of as-deposited film by AD, further investigation about the influence of particle size and morphology of raw materials on the microstructure and property of the film should be necessary. However, our present work indicates that AD method can potentially be used in the fabrication of all solid state thin film lithium-ion batteries.

## 4. Conclusion

$Li_4Ti_5O_{12}$ (LTO) thin film electrode was successfully fabricated at room temperature condition by aerosol deposition (AD) method. Agglomerated LTO powder with size of 5–6 μm composed of primary sub-micron particles was used as raw material and deposited directly on a stainless steel substrate via room temperature impact consolidation. It is worth to note that as-deposited LTO film has a same crystalline structure with raw powder and a little porous microstructure consisted from fractured LTO particles with sizes of several tens to hundred nm. LTO film electrode by AD showed good electrochemical property in liquid electrolyte. The discharge capacities of 159 mAh $g^{-1}$ and 130 mAh $g^{-1}$ were confirmed at current density of 0.067 mA $cm^{-2}$ (= 0.5C) and 2.68 mA $cm^{-2}$ (= 20C), respectively. The film electrode also showed excellent capacity retention. The results indicate that AD method can potentially be used in the fabrication of all solid state thin film lithium ion batteries.

**Acknowledgements**

The authors gratefully acknowledge for Drs. Mitsuteru Inoue and Hiroyuki Takagi in Toyohashi University of Technology for their technical advises for using the aerosol deposition apparatus. This work was partly supported by Research Grant (General Research) from TEPCO Memorial Foundation.

**References**

[1] J.B. Bates, N.J. Dudney, B. Neudecker, A. Ueda, C.D. Evans, Solid State Ionics **135** (2000) 33–45.

[2] H. Ohtsuka, Y. Sakurai, Solid State Ionics **144** (2001) 59–64.

[3] N.J. Dudney, Mat. Sci. Eng. B **116** (2005) 245–249.

[4] A. Patil, V. Patil, D.W. Shin, J.W. Choi, D.S. Paik, S.-J. Yoon, Mat. Res. Bull. **43** (2008) 1913–1942.

[5] F. Sauvage, E. Baudrin, L. Gengembre, J.M. Tarascon, Solid State Ionics **176** (2005) 1869–1876.

[6] F. Sauvage, E. Baudrin, L. Laffont, J.M. Tarascon, Solid State Ionics **178** (2007) 145–152.

[7] J.P. Sun, K. Tang, X.Q. Yu, H. Li, X.J. Huang, Thin Solid Films **517** (2009) 2618–2622.

[8] V. Palomares, I. Ruiz de Larramendi, J. Alonso, M. Bengoechea, A. Goñi, O. Miguel, T. Rojo, Appl. Surf. Sci. **256** (2010) 2563–2568.

[9] H. Xia, Y.S. Meng, L. Lu, G. Cedera, J. Electrochem. Soc. 154 (2007) A737–A743.

[10] J. Deng, Z. Lua, I. Belharouak, K. Amine, C.Y. Chung, J. Power Sources **193**

(2009) 816–821.

[11] M. Hirayama, K. Kim, T. Toujigamori, W. Cho, R. Kanno, Dalton Trans. **40** (2011) 2882−2887.

[12] K.F. Chiu, J. Electrochem. Soc. 154 (2007) A129−A133.

[13] K.F. Chiu, P.Y. Chen, Surf. Coat. Technol. 203 (2008) 872–875.

[14] X.J. Zhu, L.B. Cheng, C.G. Wang, Z.P. Guo, P. Zhang, G.D. Du, H.K. Liu, J. Phys. Chem. C 113 (2009) 14518−14522.

[15] J. Xie, N. Imanishi, T. Zhang, A. Hirano, Y. Takeda, O. Yamamoto, Electrochimica Acta 54 (2009) 4631−4637.

[16] K.F. Chiu, C.C. Chen, M.H. Chiang, W.H. Ho, J. Electrochem. Soc. **157** (2010) A130−A135.

[17] C. Wang, Y.C. Liao, F.C. Hsu, N.H. Tai, M.K. Wu, J. Electrochem. Soc. 152 (2005) A653−A657.

[18] F. Wunde, F. Berkemeier, G. Schmitz, J. Power Sources 215 (2012) 109−115.

[19] M. Mohamedi, M. Makino, K. Dokko, T. Itoh, I. Uchida, Electrochimica Acta 48 (2002) 79–84.

[20] J. Ma, Q.Z. Qin, J. Power Sources 148 (2005) 66−71.

[21] Y. Yu, J.L. Shui, C.H. Chen, Solid State. Commun. 135 (2005) 485–489.

[22] J. Akedo, J. Am. Ceram. Soc. 89 (2006) 1834−1839.

[23] J. Akedo, M. Lebedev, Appl. Phys. Lett. 77 (2000) 1710.

[24] M. Lebedev, J. Akedo, Jpn. J. Appl. Phys. 41-11B (2002) 6669–6673.

[25] J.H. Ryu, J. J. Choi, B.D. Hahn, D.S. Park, W.H. Yoon, and K.-H. Kim, Appl. Phys. Lett. 90 (2007) 152901.

[26] J.H. Ryu, D.S. Park, B.D. Hahn, J.J. Choi, W.H. Yoon, K.Y. Kim, H.S. Yun, Appl. Catal. B Environ. 83 (2008) 1–7.

[27] W.H. Yoon, J. Ryu, J.J. Choi, B.D. Hahn, J.H. Choi, B.K. Lee, J.H. Cho, D.S. Park, J. Am. Ceram. Soc. 93 (2010) 2125–2127.

[28] D. Popovici, H. Nagai, S. Fujisima, J. Akedo, J. Am. Ceram. Soc. 94 (2011) 3847–3850.

[29] H. Usui, H. Nishinami, T. Iida, H. Sakaguchi, Electrochemistry 76 (2008) 329–331.

[30] H. Usui, Y. Kashiwa, T. Iida, H. Sakaguchi, J. Power Sources 195 (2010) 3649–3654.

[31] H. Usui, M. Shibata, K. Nakai, H. Sakaguchi, J. Power Sources 196 (2011) 2143–2148.

[32] H. Usui, Y. Yamamoto, K. Yoshiyama, T. Itoh, H. Sakaguchi, J. Power Sources 196 (2011) 3911–3915.

[33] S. Takai, H. Sakaguchi, K. Tanaka, Y. Nagao, T. Esaka, Electrochemistry 76 (2008) 293–296.

[34] I. Kim, T.H. Nam, K.W. Kim, J.H. Ahn, D.-S. Park, C. Ahn, B.S. Chun, G. Wang, H.J. Ahn, Nanoscale Res. Lett. 7 (2012) 64.

[35] I. Kim, J. Park, T.H. Nam, K.W. Kim, J.H. Ahn, D.S. Park, C. Ahn, G. Wang, H.J. Ahn, J. Power. Sources 244 (2013) 646–651.

[36] T. Ohzuku, A. Ueda, N. Yamamoto, J. Electrochem. Soc. **142** (1995) 1431–1435.

[37] D. Yoshikawa, Y. Kadoma, J.M. Kim, K. Ui, N. Kumagai, N. Kitamura, Y. Idemoto, Electrochimica Acta **55** (2010) 1872–1879.

[38] M-S. Song, A. Benayad, Y-M. Choia, K-S. Park, Chem. Commun. **48** (2011)

516–518.

[39] Y. Ryo, K. Kanamura, J. Solid. State. Chem. 177 (2004) 2094–2100.

[40] J. Mosa, J.F. Vélez, I. Lorite, N. Arconada, M. Aparicio, J. Power Sources 205 (2012) 491–494.

[41] Y. Zhao. G. Liu, L. Liu, Z. Jiang, J. Solid State Electrochem. 13 (2009) 705–711.

[42] Company website: http://www.iskweb.co.jp/eng/products/battery.html.

## Figure captions

**Fig. 1**. A schematic illustration of the apparatus for aerosol deposition.

**Fig. 2**. SEM image of commercial $Li_4Ti_5O_{12}$ powder used as a raw material for film deposition. Enlarged image of surface morphology of the powder is also shown.

**Fig. 3**. Particle size distribution of commercial $Li_4Ti_5O_{12}$ powder used as raw material for fabrication of $Li_4Ti_5O_{12}$ film by AD.

**Fig. 4**. XRD patterns for $Li_4Ti_5O_{12}$ powder used as raw material (top) and as-deposited $Li_4Ti_5O_{12}$ film on stainless steel substrate by AD (bottom).

**Fig. 5**. Enlarged (111) diffraction peaks of raw $Li_4Ti_5O_{12}$ powder (top) and as-deposited $Li_4Ti_5O_{12}$ film by AD (bottom).

**Fig. 6**. SEM image of the fractured cross section for as-deposited $Li_4Ti_5O_{12}$ film on stainless steel substrate. Enlarged image of cross section of the film is also shown.

**Fig. 7**. Charge and discharge curves of as-deposited $Li_4Ti_5O_{12}$ film electrode by AD at 20°C and different fixed current density of 0.067, 0.268, 0.536, 1.34 and 2.68 mA $cm^{-2}$. Note that the current density of 0.134 mA $cm^{-2}$ is corresponding to 1C rate.

**Fig. 8**. Rate performance of discharge capacity for as-deposited $Li_4Ti_5O_{12}$ film electrode by AD. Note that the current density of 0.134 mA $cm^{-2}$ is corresponding to 1C rate.

**Fig. 9**. Discharge capacity (a) and coulombic efficiency (b) of as-deposited $Li_4Ti_5O_{12}$ film electrode by AD at current density of 0.134 mA $cm^{-2}$ (= 1C) plotted against cycle number.

**Fig. 10**. Discharge capacity (a) and coulombic efficiency (b) of as-deposited $Li_4Ti_5O_{12}$ film electrode by AD at current density of 0.536 mA $cm^{-2}$ (= 4C) plotted against cycle number. Note that this measurement was carried out after the measurement at current density of 0.134 mA $cm^{-2}$ (= 1C) shown in Fig. 9.

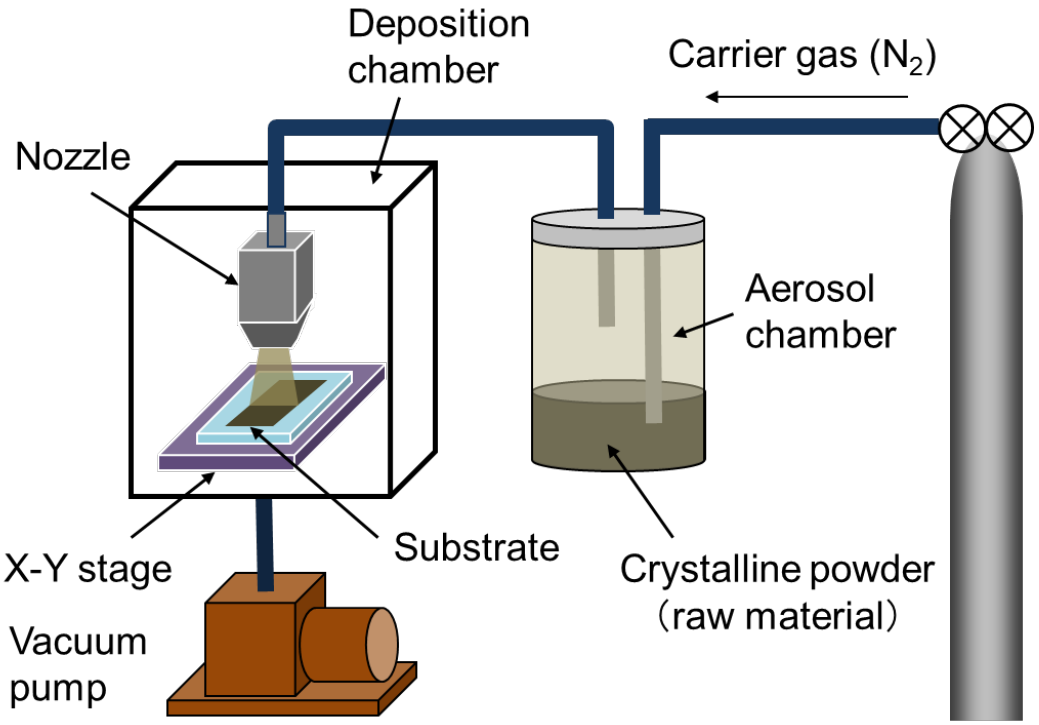
Deposition
chamber
Carrier gas ($N_2$)
Nozzle
Aerosol
chamber
X-Y stage
Substrate
Crystalline powder
(raw material)
Vacuum
pump

**Fig. 1**

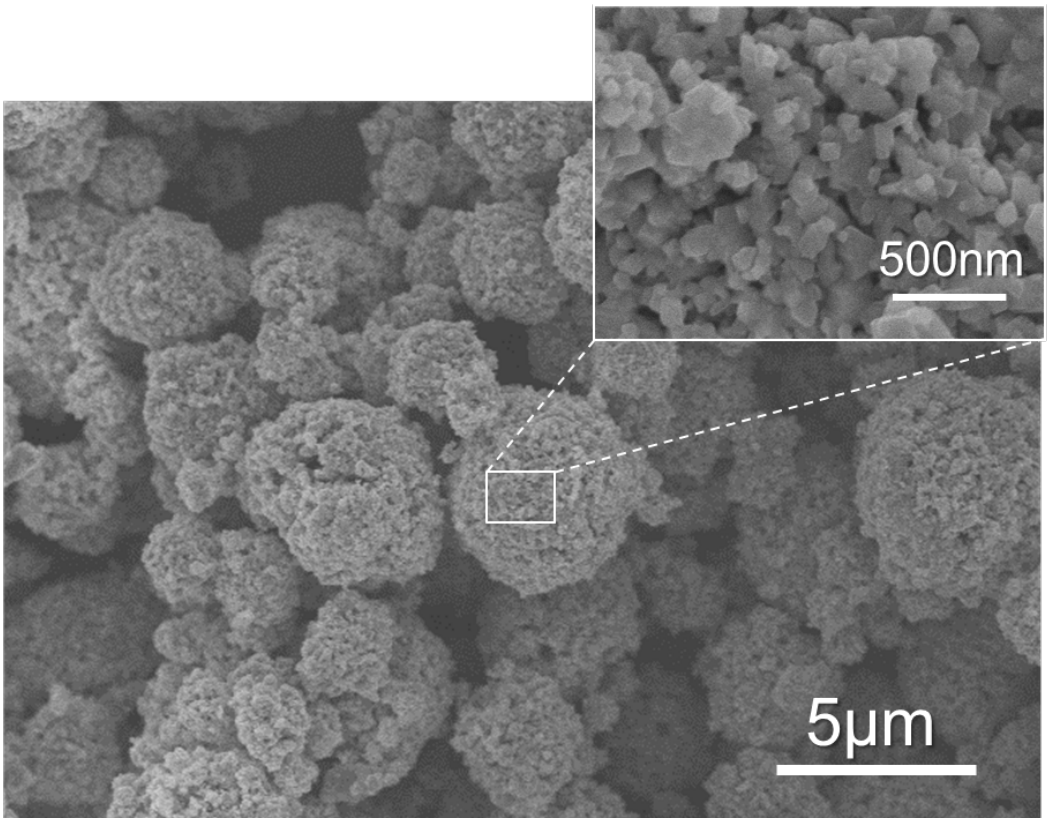


**Fig. 2**

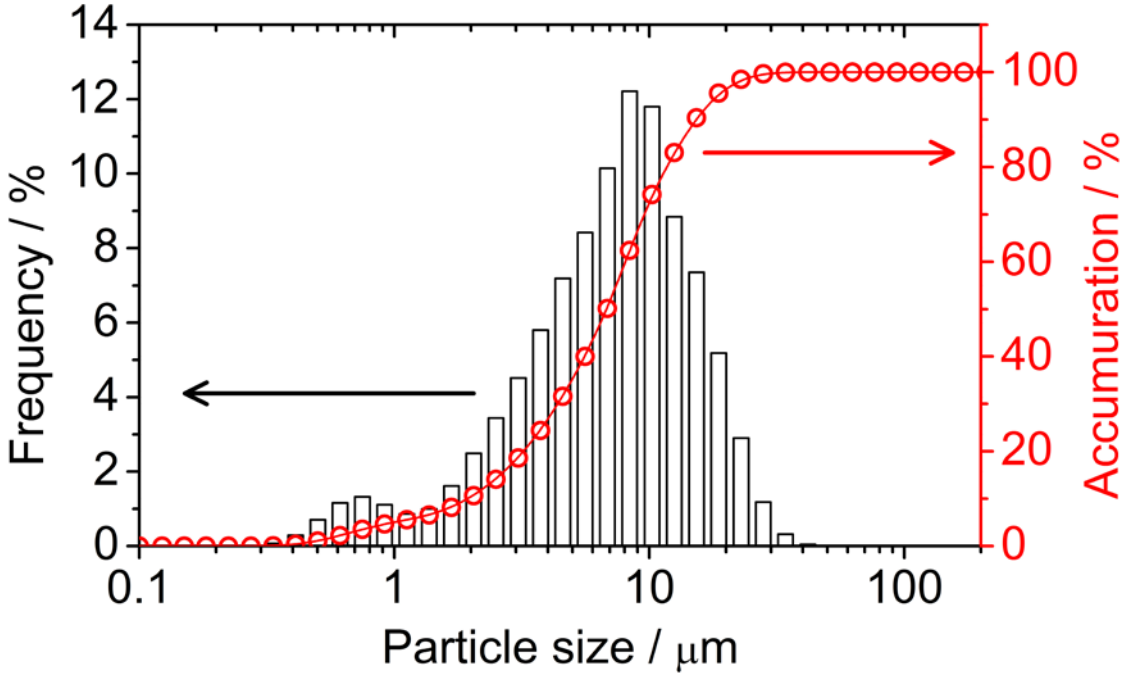
Frequency / %
Accumuration / %
Particle size / μm
0
2
4
6
8
10
12
14
0
20
40
60
80
100
0.1
1
10
100

**Fig. 3**

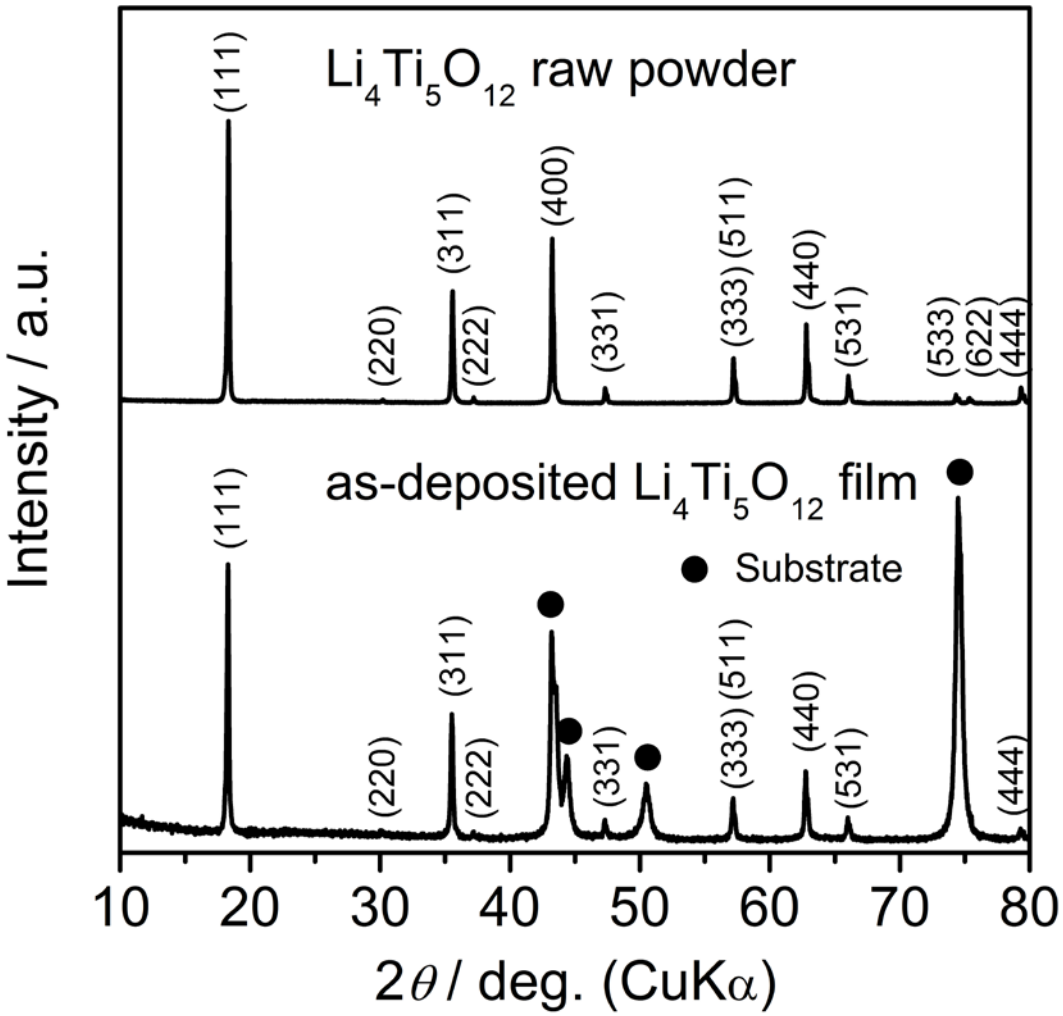
Li4Ti5O12 raw powder
(111)
(220)
(311)
(222)
(400)
(331)
(333) (511)
(440)
(531)
(533)
(622)
(444)
as-deposited Li4Ti5O12 film
Substrate
(111)
(220)
(311)
(222)
(331)
(333) (511)
(440)
(531)
(444)
Intensity / a.u.
10
20
30
40
50
60
70
80
2θ / deg. (CuKα)

**Fig. 4**

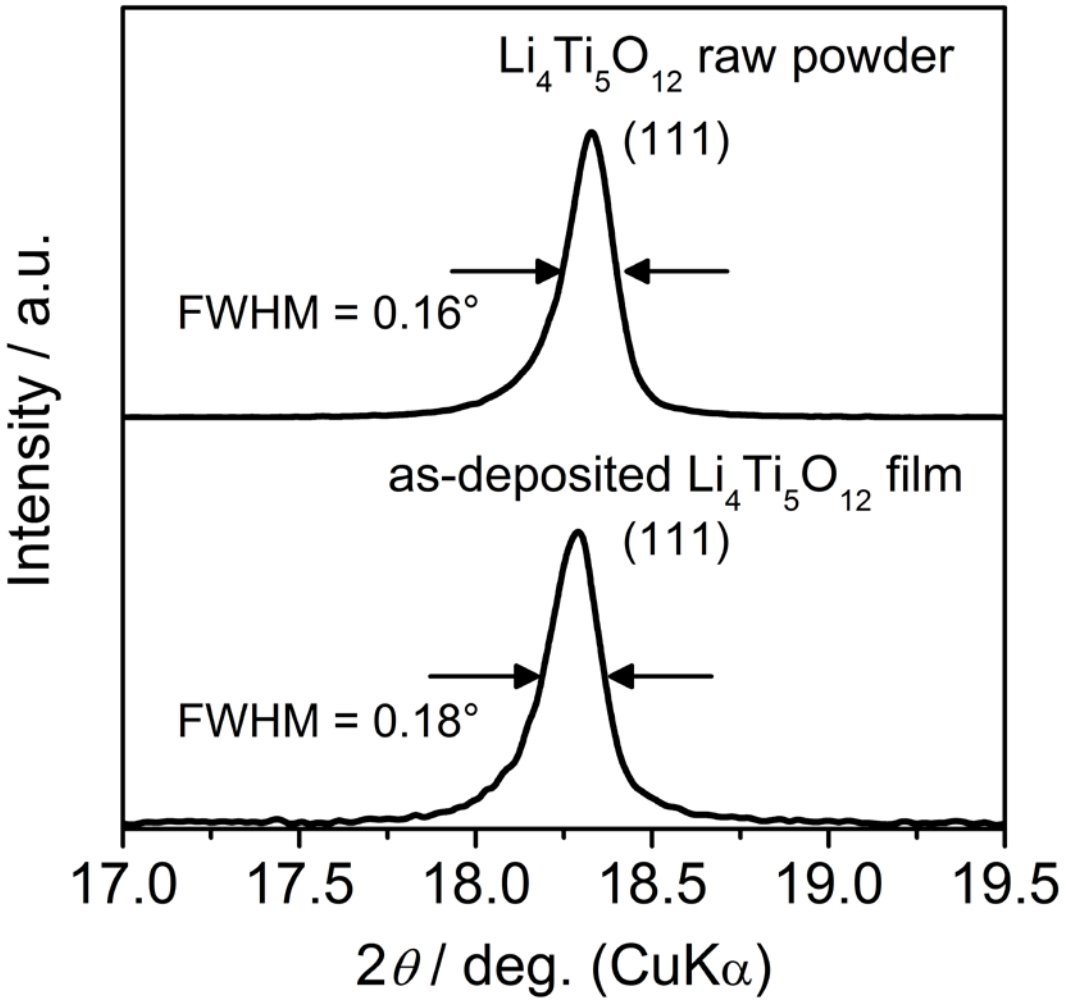
Li4Ti5O12 raw powder
(111)
FWHM = 0.16°
as-deposited Li4Ti5O12 film
(111)
FWHM = 0.18°
Intensity / a.u.
17.0
17.5
18.0
18.5
19.0
19.5
2θ / deg. (CuKα)

**Fig. 5**

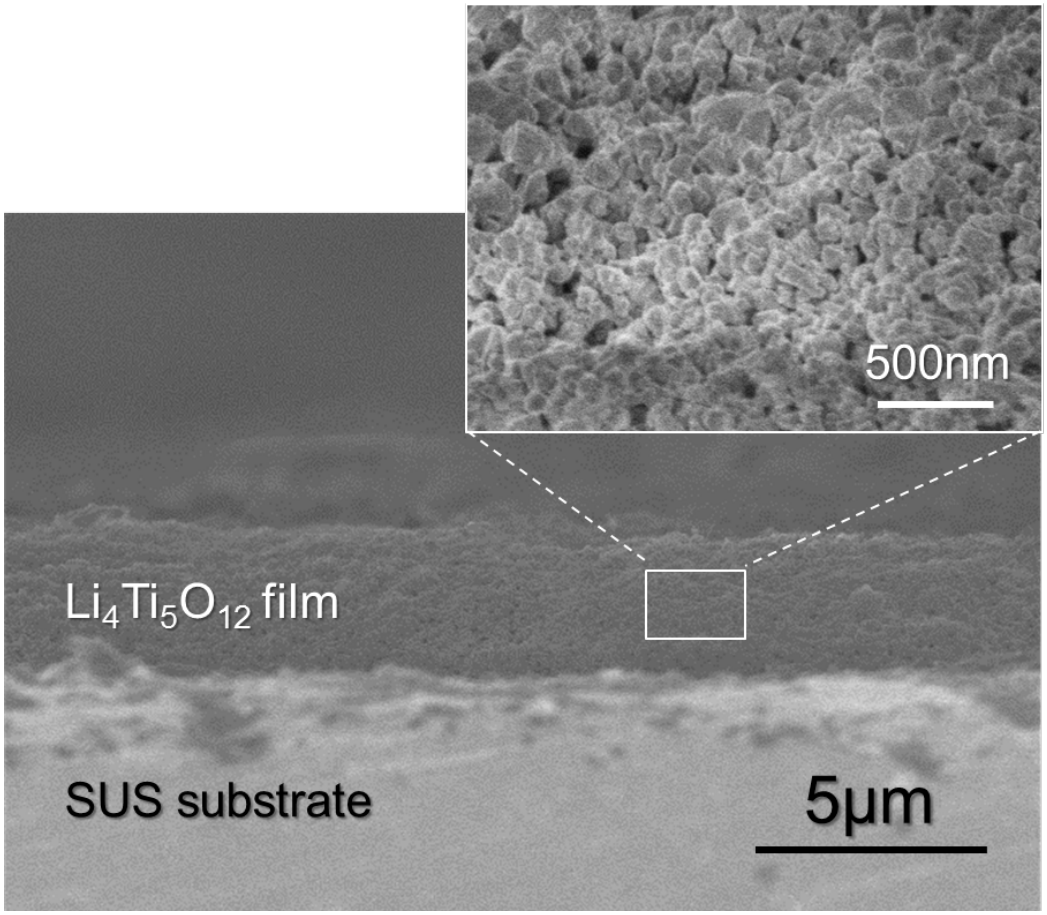


**Fig. 6**

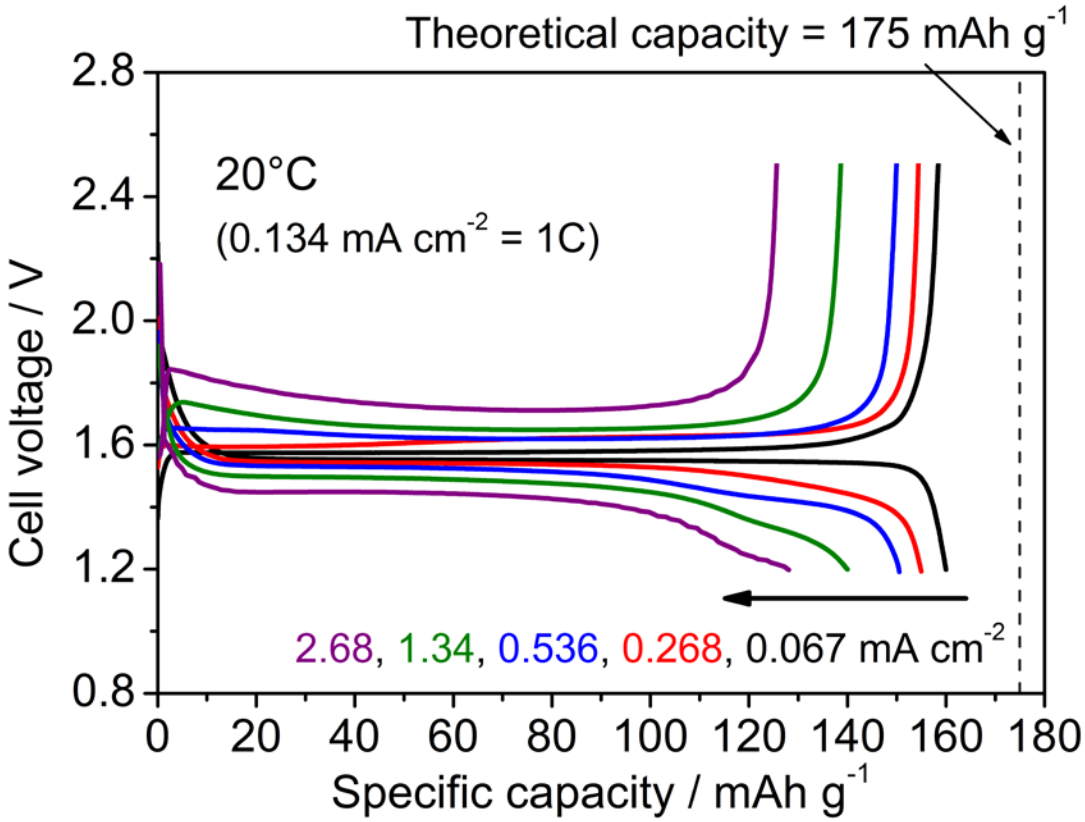
Theoretical capacity = 175 mAh g-1
20°C
(0.134 mA cm-2 = 1C)
2.68, 1.34, 0.536, 0.268, 0.067 mA cm-2
Cell voltage / V
Specific capacity / mAh g-1
2.8
2.4
2.0
1.6
1.2
0.8
0
20
40
60
80
100
120
140
160
180

**Fig. 7**

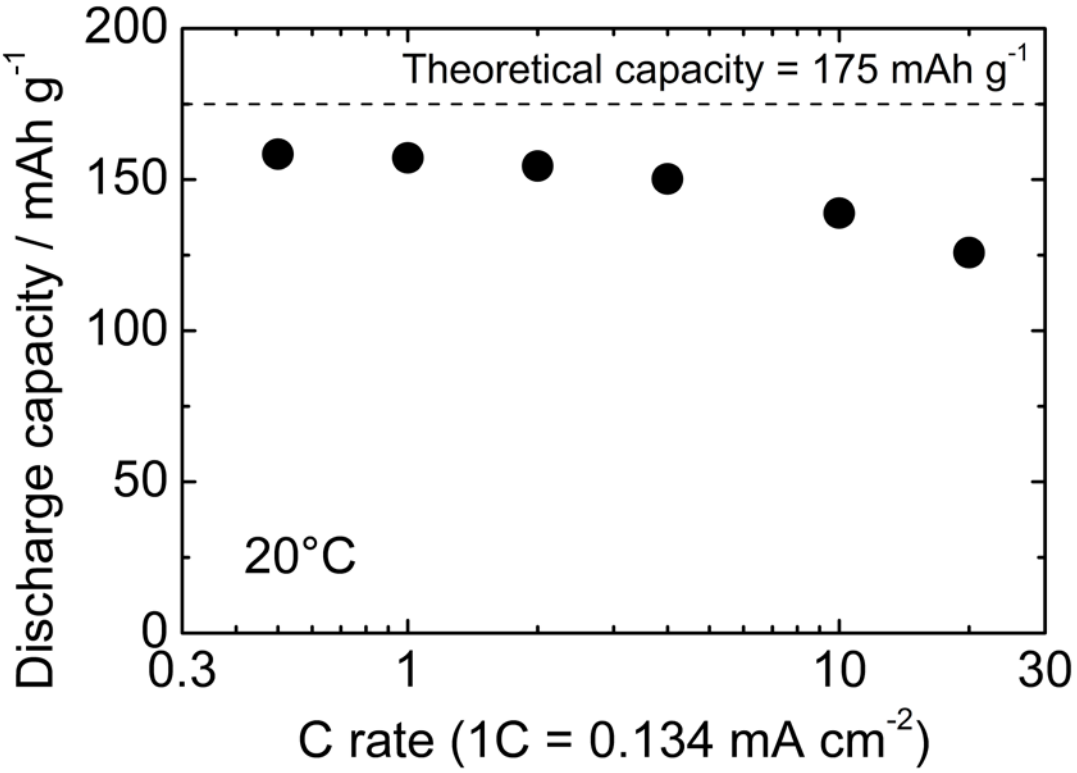
Theoretical capacity = 175 mAh g-1
Discharge capacity / mAh g-1
200
150
100
50
0
20°C
0.3
1
10
30
C rate (1C = 0.134 mA cm-2)

**Fig. 8**

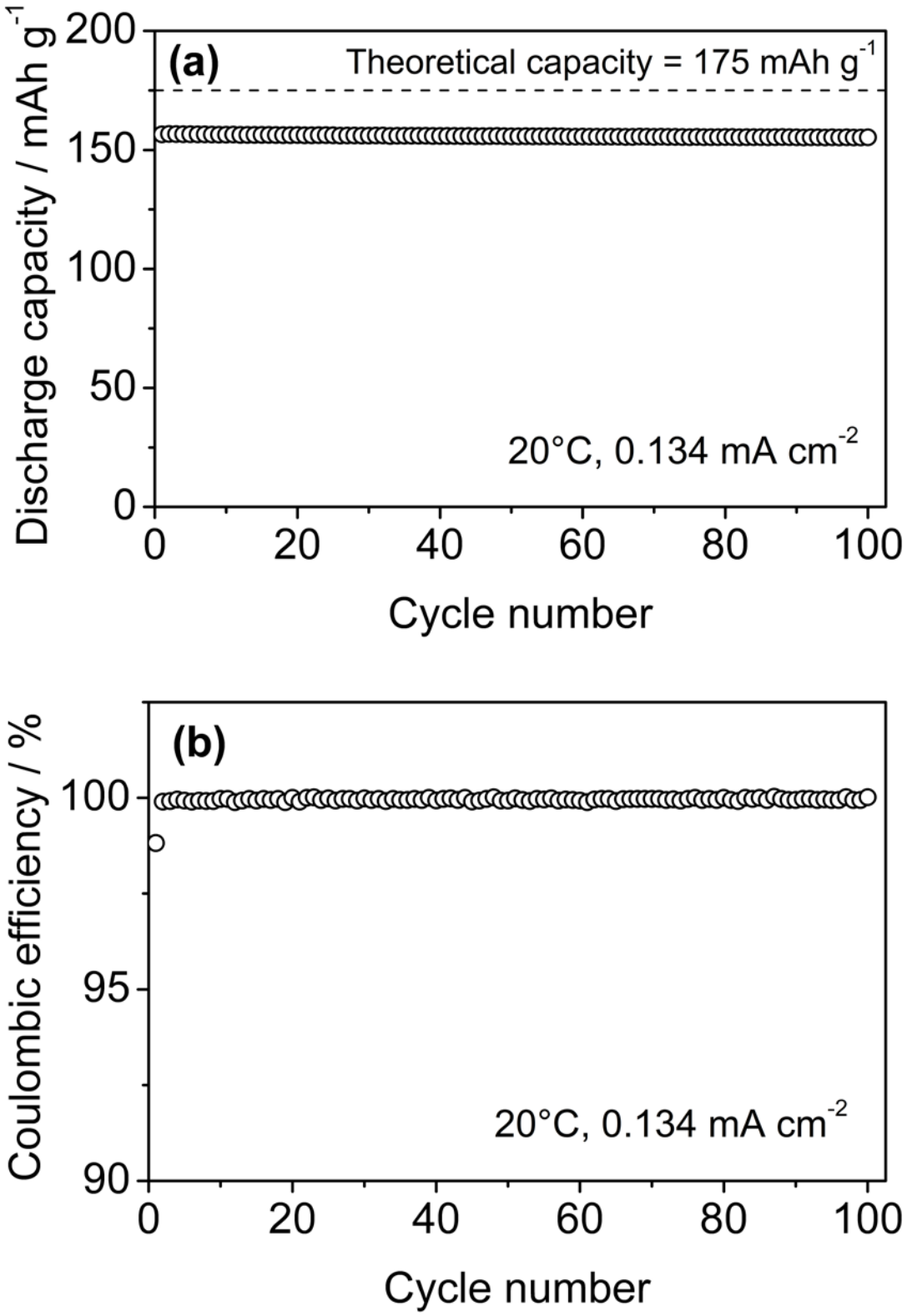
(a)
Theoretical capacity = 175 mAh g-1
20°C, 0.134 mA cm-2
Discharge capacity / mAh g-1
Cycle number
(b)
20°C, 0.134 mA cm-2
Coulombic efficiency / %
Cycle number

**Fig. 9**

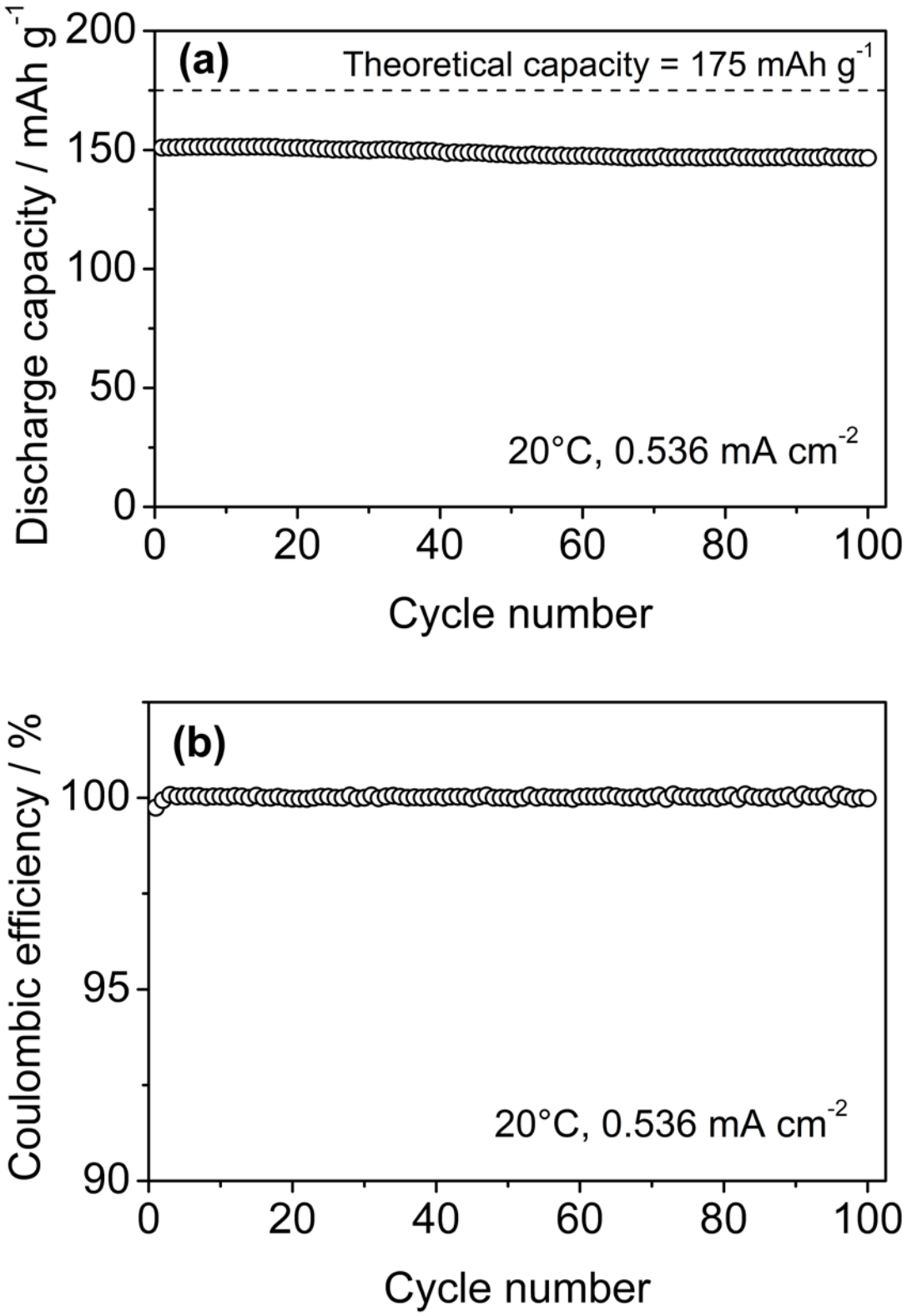
(a)
Theoretical capacity = 175 mAh g-1
Discharge capacity / mAh g-1
200
150
100
50
0
20°C, 0.536 mA cm-2
0
20
40
60
80
100
Cycle number
(b)
Coulombic efficiency / %
100
95
90
20°C, 0.536 mA cm-2
0
20
40
60
80
100
Cycle number

**Fig. 10**